Journal of
Synchrotron Radiation

ISSN 0909-0495

Received 8 September 2009
Accepted 21 December 2009

Application of kinoform lens for X-ray reflectivity analysis

M. K. Tiwari,* L. Alianelli, I. P. Dolbnya and K. J. S. Sawhney

Diamond Light Source Ltd, Harwell Science and Innovation Campus, Didcot, Oxfordshire OX11 0DE, UK. E-mail: manoj.tiwari@diamond.ac.uk

In this paper the first practical application of kinoform lenses for the X-ray reflectivity characterization of thin layered materials is demonstrated. The focused X-ray beam generated from a kinoform lens, a line of nominal size $\sim$50 μm × 2 μm, provides a unique possibility to measure the X-ray reflectivities of thin layered materials in sample scanning mode. Moreover, the small footprint of the X-ray beam, generated on the sample surface at grazing incidence angles, enables one to measure the absolute X-ray reflectivities. This approach has been tested by analyzing a few thin multilayer structures. The advantages achieved over the conventional X-ray reflectivity technique are discussed and demonstrated by measurements.

Keywords: kinoform lens; X-ray reflectivity; thin multilayer structures; synchrotron radiation source.

1. Introduction

X-ray reflectivity (XRR) is a widely used technique for surface–interface characterization of thin films and X-ray multilayer structures, deposited on substrate surfaces. A multilayer structure consists of thin layers of alternating elements or compounds (Spiller, 1972; Barbee, 1985). These thin film structures offer unique structural (Windt *et al.*, 2003), magnetic (Wellock *et al.*, 1999; Costa Jr *et al.*, 2001) and electronic (Zahn *et al.*, 2002; Revaz *et al.*, 2002) properties with a wide range of applications. Multilayers as an X-ray optical element are used in many technological applications like X-ray astronomy, microscopy and spectroscopy. They are also employed as filters and monochromators in synchrotron radiation and free-electron X-ray lasers. In XRR, the requirement of glancing incidence angle for the incoming X-ray beam, on the sample surface, imposes a constraint for the maximum allowable vertical size of the incoming X-ray beam. Usually, a line-shaped X-ray beam with a vertical size of $\sim$20–50 μm and a horizontal size of $\sim$2–10 mm is used for the XRR measurements. Such a micrometre-size beam is generated by slitting down the primary beam, which however reduces the incident flux. The XRR technique has a limitation: it cannot be applied for sample scanning analysis mode because of the large footprint of the X-ray beam generated on the sample surface at grazing incidence angles.

Focused X-ray beams produced from various focusing optics such as Kirkpatrick–Baez optics, Fresnel zone plate, capillary optics, nano-collimators and X-ray waveguide structures have been used in many applications such as X-ray fluorescence microscopy, microtomography, X-ray imaging and scattering measurements (Jark *et al.*, 2001; Lagomarsino *et al.*, 1997; Di Fonzo *et al.*, 2000; Zwanenburg *et al.*, 1999; Cedola *et al.*, 2003). It has been shown that the X-ray beams generated from compound refractive lens optics can be successfully employed for X-ray standing-wave fluorescence scanning microscopy applications (Drakopoulos *et al.*, 2002) and for X-ray characterization of deeply buried interface structures (Reichert *et al.*, 2003). The applicability of microfocused synchrotron X-ray beams seems to be very useful especially for investigating the structural properties of heterogeneous thin film structures (Wolkenhauer *et al.*, 2006; Matsui *et al.*, 2007). Focusing, of course, increases the beam divergence, which can be a drawback for some techniques. In the case of the XRR technique, however, it has already been shown (Tiwari *et al.*, 2007) that the primary beam divergence effect can easily be taken into account in the model calculation while fitting the experimental XRR data.

A kinoform lens is a one-dimensional X-ray focusing optics that generates a line-focused X-ray beam of vertical size typically $\sim$0.5–3 μm (Evans-Lutterodt *et al.*, 2003; Stein *et al.*, 2008; Alianelli *et al.*, 2009). The kinoform lenses are based on refraction and work in a similar way to compound refractive lenses (CRLs) (Snigirev *et al.*, 1996). The absorption losses in a kinoform lens are significantly lower compared with CRLs. These structures are usually characterized by very high X-ray transmission efficiencies (theoretical transmission $\sim$90%) especially at mid-to-high X-ray energies (6–20 keV). Furthermore, the possibility of fabricating them with very small radius of curvature makes it possible to use only a single lens system for short focal length applications rather than using a stack of several lenses as in CRLs. With recent technological advances, it has now become possible to fabricate kinoform lenses with larger effective aperture in the range

200–400 µm (Alianelli *et al.*, 2007; Isakovic *et al.*, 2009), making them suitable for use in real synchrotron applications.

At Diamond, a program has already been started to design, fabricate and test in-line refractive optics made by micro-fabrication techniques and to use them for real synchrotron applications. In a previous work (Alianelli *et al.*, 2009), we have described the fabrication and testing of the focusing properties of Si and Ge kinoform lenses using X-rays originating from a bending-magnet source (Sawhney *et al.*, 2009). In the present work, we demonstrate the first practical application of the kinoform lenses for XRR characterization of thin layered materials. We have used Si kinoform lenses fabricated at Diamond Light Source (Alianelli *et al.*, 2009) for the XRR characterization of Nb/C/Nb and Mo/Si multilayer structures. We show that the one-dimensional focusing properties of the kinoform lenses make them ideal for the XRR measurements. Moreover, the small beam footprint generated on the sample surface, even at shallow glancing incidence angles, provides the possibility to perform the XRR measurements in sample scanning mode, and also enables the absolute reflectance to be measured.

2. Experimental

The measurements were performed on the B16 Test beamline at the Diamond Light Source (Sawhney *et al.*, 2009). B16 Test beamline is a bending-magnet-based beamline and has an acceptance of 3 mrad (h) × 0.5 mrad (v). It works over the 2–25 keV photon energy range. The main optical components of the beamline are a Si(111) double-crystal monochromator (DCM), a toroidal mirror and a double-multilayer monochromator (presently under construction). The DCM is placed 20 m away from the source, and the toroidal mirror is placed 2 m downstream of the DCM. The toroidal mirror provides focusing in both planes and is employed with 1:1 focusing geometry. The beamline has two main experimental stations: (i) a medium heavy-duty five-axis Huber diffractometer and (ii) a versatile Optics test bench, which offers several degrees of motion. These experimental stations were placed at a distance of 44 m and 47 m from the source, respectively. For the measurement reported here, we used unfocused monochromatic X-rays in the energy range 10–20 keV, selected by the DCM. The XRR measurements were performed on the five-axis Huber diffractometer in θ–2θ geometry. The thin film samples were installed on the sample stage of the diffractometer, which consisted of three (XYZ) precision motorized stages. These stages facilitate the alignment of the thin film samples with accuracies better than 1 µm. We also employed an optical microscope for preliminary visual alignment of the samples; however, the final alignment of the samples was carried out using X-rays. The measured 'sphere of confusion' of the diffractometer station over the full range of all five axes, with a sample load of 20 kg, was found to be better than 60 µm. The 'circle of confusion' for the two axes (θ and 2θ) used here was found to be close to 3 µm for incidence angle variations of 0–10°. The angular resolution of both θ and 2θ motions was better than 0.5 mdeg. The XRR scans of the thin film samples were performed for incidence angles ranging from 0 to 3°. To measure specular reflected X-ray intensity from the sample, an avalanche photodiode detector capable of measuring very high count rates and having a large dynamic range was employed.

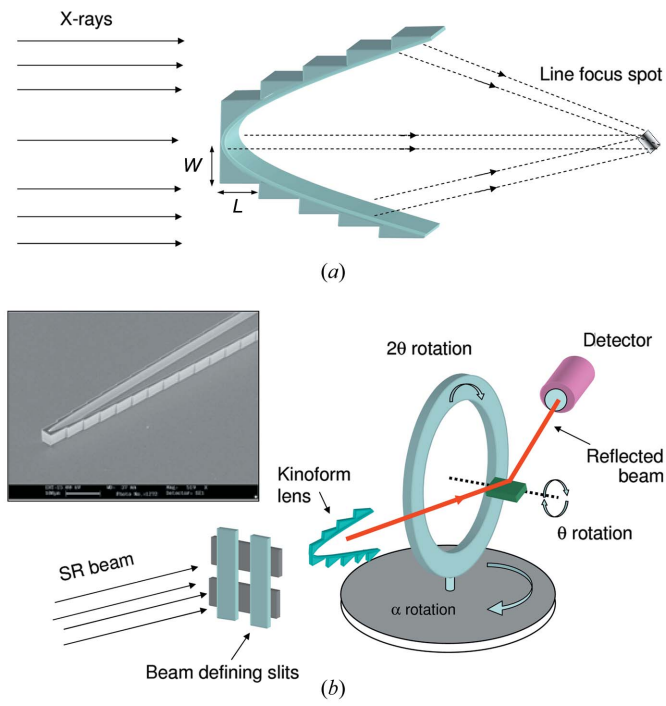

Figure 1
(*a*) Schematic view of the focusing of X-rays from a planar kinoform single-element lens. The step length L is given by the ratio of the incident wavelength to the refractive index decrement of the lens material ($L = \lambda/\delta$). The width W depends on the aperture of the lens. The kinoform lens generates a line-focus X-ray beam of nominal size ∼50 µm × 2 µm. (*b*) Schematic of the XRR arrangement using a focused X-ray beam generated from a kinoform lens structure. The inset shows a scanning electron micrograph of the Si kinoform lens structure.

Fig. 1(*a*) shows a schematic view of the focusing of X-rays using a kinoform lens. The lens generates a line focus X-ray spot at the focal distance of the lens. The step length L depends on the incident X-ray wavelength λ and on the real part of the refractive index δ of the lens material ($L = \lambda/\delta$). The step width W usually depends on the lens aperture. Its value decreases with increasing lens aperture. At the centre of the lens, the value of W ranges by a few micrometres. The experimental arrangement for the XRR measurements is shown in Fig. 1(*b*), and a scanning electron micrograph image of the kinoform lens is shown in the inset. The lens–sample distance was kept equal to the focal length of the lens. The kinoform lens structures, fabricated side-by-side on a Si substrate chip, were mounted on an attocube (http://www.attocube.com/) tower having five degrees of motion, which in turn was placed on the incident arm of the Huber diffractometer. Fig. 2 shows photographs of the experimental set-up.

The attocube stages provide great flexibility in aligning the kinoform lens as well as bringing a specific designed lens into the X-ray beam path at a designed X-ray energy. Before the kinoform lens structure, a four-blade beam-defining slit was

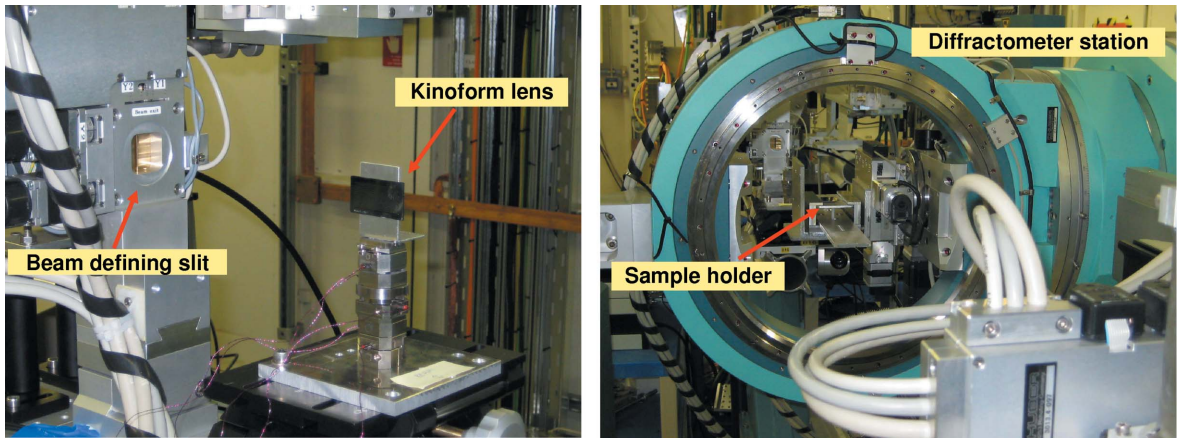

Figure 2
Photographs of the experimental set-up showing the arrangement of the XRR measurement using a Si kinoform lens. The kinoform lens structures were mounted on an attocube tower having five degrees of motion. The beam-defining slits were mounted upstream of the kinoform lens optics.

mounted, which allowed us to match the size of the X-ray beam with the exact aperture of the kinoform lens. The kinoform lens was aligned in the X-ray beam by observing the focused beam on an area CCD detector (Photonic Sciences) that has an effective pixel size of 6.5 µm. The focal distance, tilt, yaw and pitch of the lens was adjusted to derive a good line-focused beam at the sample position. After this initial alignment, the size of the focused beam at the sample position was determined by a wire scan measurement, using a 200 µm-diameter Au wire.

The Nb/C/Nb trilayer and Mo/Si multilayer structures employed in this study were fabricated using a DC magnetron sputtering system (Lodha, 2009). The thin film structures were deposited on Si (100) substrates, which were held at room temperature during the deposition. Before deposition, the r.m.s. roughness of the Si substrates was determined using XRR measurements on a laboratory-source-based reflectometer and was found to be 5 ± 1 Å.

3. Results and discussion

Fig. 3 shows the X-ray images of the kinoform lens structures recorded using the X-ray CCD camera. Measuring at incident X-ray energy close to 19 keV, Figs. 3(*a*), 3(*b*) and 3(*c*), respectively, show images of a few lens structures, a single lens structure, and a single lens structure under conditions of reduced primary beam size. These images were collected at a distance of ∼580 mm (equal to the focal length) from the lens apex. The beam-defining slits were used to generate a primary X-ray beam size that matches exactly the effective aperture of the kinoform lens structure. For example, the vertical size of the primary beam-defining slit was set in the range ∼100–200 µm in order to select the full effective aperture of a kinoform lens structure at a given X-ray energy. From Fig. 3(*c*) it can be seen that by properly selecting the primary beam aperture a line-shaped X-ray beam of size ∼50 µm (h) × 2 µm can be generated. The vertical size of the focused X-ray beam was measured with better accuracy using a wire scan. Fig. 4 shows the measured vertical size of the focused X-ray beam

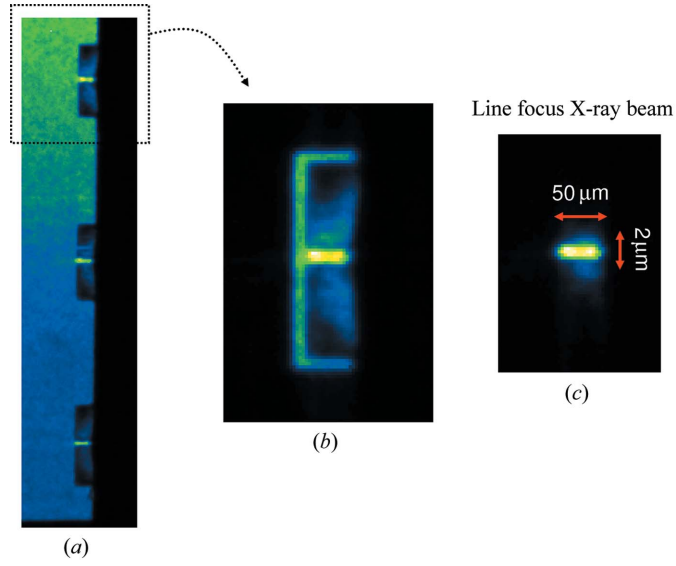

Figure 3
Recorded X-ray images of the Si kinoform lens structures at an incident X-ray energy of 19 keV. (*a*) Image of a few lenses, (*b*) a single lens and (*c*) a single lens after defining the primary X-ray beam size equal to the lens aperture. From (*c*) it can be seen that the kinoform lens generates a well defined line-shaped X-ray beam of size 50 µm × 2 µm. In (*b*) and (*c*), the vertical size of the X-ray beam was set to ∼140 µm and 90 µm, respectively, using a beam-defining slit as shown in Fig. 2.

at the sample position, under conditions corresponding to Fig. 3(*c*). This vertical size of the focused X-ray beam was derived by taking the derivative of the raw wire scan data, as shown in the inset of Fig. 4. The vertical size of the focused X-ray spot was found to be ∼2 µm (FWHM). The horizontal size of the focused beam usually depends on the depth of the lens structure on the Si substrate; in our case it was ∼50 µm.

Fig. 5 shows the measured XRR profile of a Mo/Si (d = 6.52 nm, Γ = 0.378 and N = 20) multilayer structure at an incident X-ray energy of 19 keV. Here, d defines the multilayer period, Γ is the thickness ratio of high-Z layer to multilayer period and N is the total number of layer pairs. In the first case, Fig. 5(*a*), the XRR profile has been measured with the focused

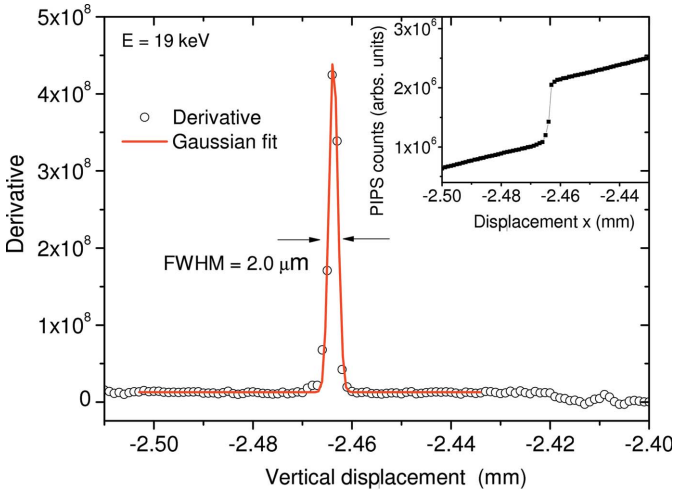

Figure 4
Wire scan measurements for the focused X-ray beam, generated from a Si kinoform structure at the sample position, under the condition corresponding to Fig. 3(*c*). The vertical size of the focused beam was determined by fitting the derivative of the raw data (as shown in the inset) and was found with a FWHM of 2 μm.

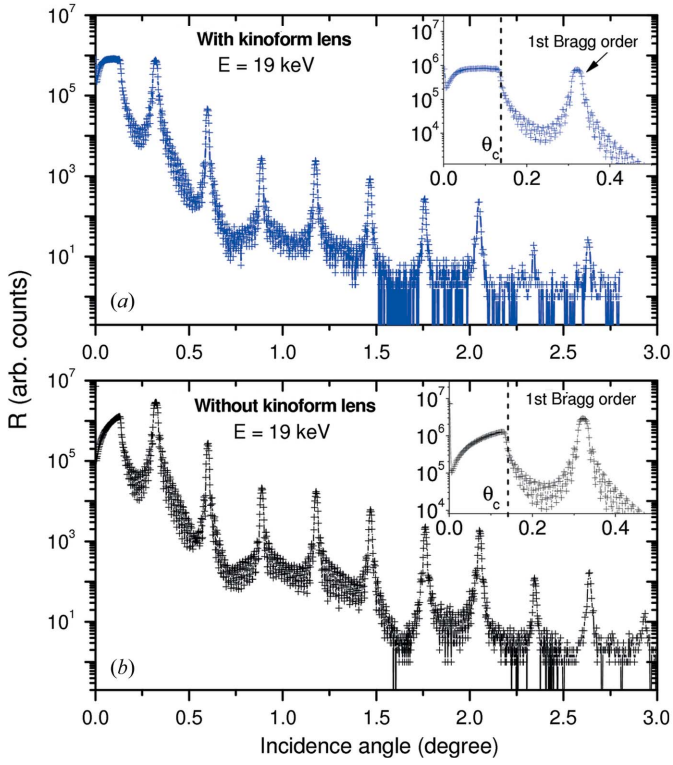

Figure 5
Measured XRR profile of a Mo/Si multilayer (d = 6.52 nm, Γ = 0.378 and N = 20) at an incident X-ray energy of 19 keV under two conditions: (*a*) using a focused X-ray beam with kinoform lens and (*b*) using an unfocused X-ray beam (kinoform lens is retracted). In both cases the experimental conditions were maintained identical, and a similar aperture of the primary X-ray beam was employed. In the insets, an extended view of XRR profiles in the vicinity of the critical angle and the first Bragg peak is shown in each case.

beam obtained from a kinoform lens structure of shape and size as shown in Fig. 3(*c*). In the second case, Fig. 5(*b*), we have measured the XRR profile with an unfocused X-ray beam under the same experimental conditions. For this, we simply retracted the kinoform lens out from the X-ray beam path. From Figs. 5(*a*) and 5(*b*), it can be seen that Bragg peaks up to nine diffraction orders are clearly visible in the measured XRR profiles. Furthermore, from these figures it can be seen that when a line-focused beam, generated from a kinoform lens, is used for the XRR measurements (Fig. 5*a*) one obtains a more or less constant reflected intensity below the critical angle of the multilayer mirror ($\theta_c = 0.136^\circ$). This flat region of XRR intensity below θ_c greatly helps in evaluating the normalized reflectance of the various Bragg peaks of a multilayer structure. On the other hand, in the case of the XRR measurements with unfocused X-ray beam (without kinoform lens) (Fig. 5*b*), one observes a strong footprint effect in the measured XRR profile. The reflected intensity below θ_c is rather less compared with the first Bragg order reflected intensity. In the insets of Fig. 5, an expanded view of the measured XRR profiles, in the vicinity of the critical angle, for the two cases is shown. For these XRR measurements, using focused (unfocused) X-ray beams, we employed a counting time of 2 s (1 s) for each angle position. Because of the presence of strong geometry effects at grazing incidence angle in the XRR measurements of Fig. 5(*b*), it is not possible to determine the normalized X-ray reflectance of various Bragg peaks of the multilayer structure or to establish the structural parameters, such as roughness, interlayer diffusion, thickness of various layers of the multilayer structure, as most of the available XRR fitting programs use normalized XRR data in their calculation scheme. To overcome this normalization problem, one normally uses a knife-edge aperture, which helps in restricting the footprint of the X-ray beam on the sample surface. However, this approach works only for the low-to-mid X-ray energy range (E = 5–12 keV) but becomes impractical if the XRR measurements are to be performed at higher X-ray energies (E > 15 keV) because of the extreme shallow grazing angles required for such high X-ray energies. For example, to restrict the footprint length of the primary X-ray beam to ∼10 mm on the sample surface at an incidence angle of 0.05°, one requires a vertical gap as small as ∼4 μm to be set between the knife and the sample surface. Clearly, it becomes difficult to make such small gaps by mechanical means alone.

The structural parameters of the Mo/Si multilayer structure such as thickness, roughness of high- and low-Z layers, and Γ ratio were determined using XRR measurements, carried out with a kinoform-focused X-ray beam (Fig. 5*a*). For fitting of the XRR data we employed a non-linear least-square fitting procedure using Parratt's formalism (Parratt, 1954). We used the optical constants (δ and β) from Henke's tabulation (http://www.cxro.lbl.gov/optical_constants/), and used deposited thickness values as the starting guess in the fitting process. Fig. 6 gives the fitted XRR profile of the Mo/Si multilayer structure along with the experimental data. The best-fit XRR results yield a thickness value of 2.47 ± 0.03 nm for the Mo layers and 4.05 ± 0.03 nm for the Si layers. The roughness of the Mo (Si) layers was found to be 0.3 nm (0.8 nm). The detailed fitting also indicated that an oxide layer of thickness

2.0 nm and roughness 0.8 nm is present on the top Si layer of the Mo/Si multilayer structure.

In another application, we have performed XRR characterization of an Nb/C/Nb trilayer structure deposited on a Si substrate. Such trilayer structures work as X-ray waveguides and they are used to compress the X-ray intensity in the mid-to-low-Z layer guiding medium. Fig. 7 shows the XRR measurements of the Nb/C/Nb trilayer structure, performed at various locations on the sample surface. For these measurements, an incident X-ray energy close to 12 keV focused from an appropriate-designed kinoform lens structure was employed. To measure the XRR profile of the trilayer structure in sample scanning mode, sample movement with a step of 2 mm was employed. Thus all the measurement locations (*e.g.* 1, 2, 3, . . . , 6 in Fig. 7) are 2 mm apart. The XRR measurements performed at various locations of the sample surface are shown in Fig. 7. The structural parameters of the Nb/C/Nb trilayer structure, at each measured location, were extracted from the best-fit XRR results. Table 1 summarizes the thickness and roughness values obtained at various locations of the sample surface. It can be seen that the obtained values of thicknesses of the individual layers of the Nb/C/Nb structure are more or less similar. Moreover, the determined r.m.s. roughness values of the three layers, as shown in parentheses in Table 1, are also found to be similar at different locations on the sample. This shows that the Nb/C/Nb layer structure is quite homogeneous. We did not observe any spatial variation in the microstructural properties of the Nb/C/Nb layer structure.

Table 1
Determined structural parameters such as thickness and roughness of the Nb/C/Nb trilayer structure from the scanning XRR measurements at different locations on the sample.

The determined r.m.s. roughness values of individual layers obtained from best-fit XRR results are shown in parentheses.

	Measured thickness and roughness at various locations on the sample surface (nm)					
	1	2	3	4	5	6
Top Nb layer	6.45 (2.5)	6.45 (2.5)	6.43 (2.5)	6.45 (2.5)	6.45 (2.5)	6.45 (2.5)
C layer	30.6 (0.9)	30.6 (0.8)	30.5 (0.9)	30.6 (0.8)	30.4 (0.8)	30.4 (0.8)
Bottom Nb layer	24.7 (1.1)	25.0 (1.2)	24.8 (1.1)	25.0 (1.3)	25.0 (1.1)	24.8 (1.3)
Si–oxide layer†	2.5 (0.4)	2.5 (0.2)	2.5 (0.2)	2.5 (0.4)	2.5 (0.2)	2.6 (0.5)

† Between bottom Nb layer and Si substrate.

The above measurements on the multilayer and the trilayer structures show that by using line-focused X-ray beams generated from a kinoform lens the XRR characterization of thin layered materials is readily possible with equal ease compared with the more conventional XRR measurement procedures of using unfocused X-ray beams and employing a knife-edge to restrict the beam footprint on the sample surface. Kinoform optics offer several merits. They have lower scattered background (especially Compton scattering)

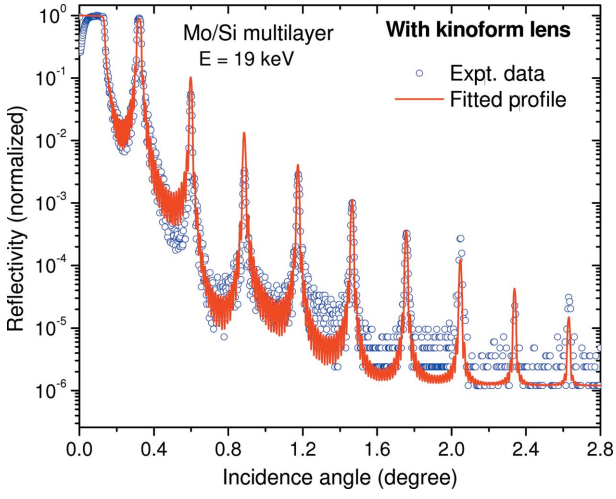

Figure 6
Fitted XRR profile of the Mo/Si multilayer structure at an incident X-ray energy of 19 keV corresponding to the measured XRR profile shown in Fig. 5(*a*). From this figure it can be seen that fitted and measured XRR profiles match quite well at lower incidence angles as well as at higher incidence angles.

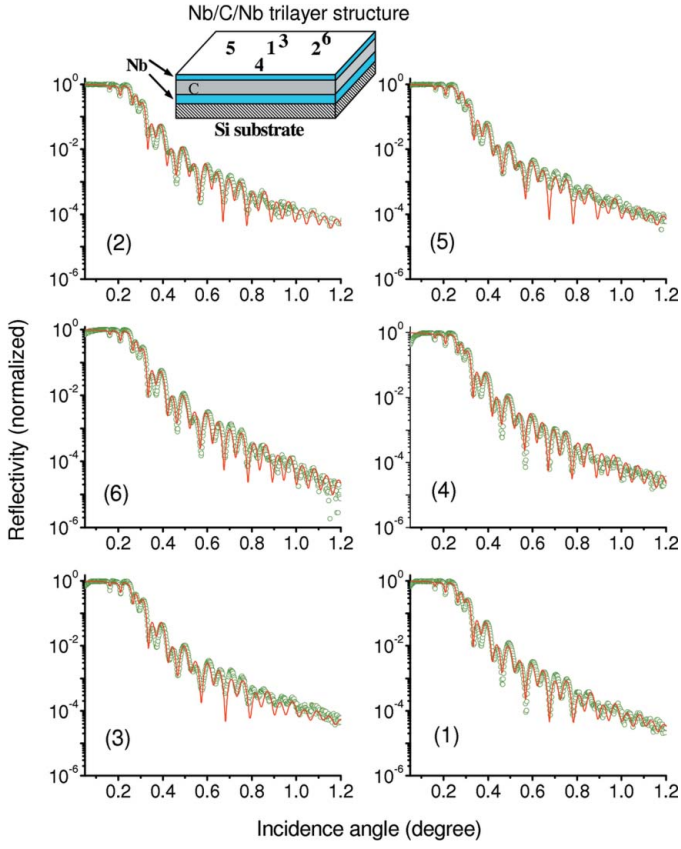

Figure 7
Measured and fitted XRR profiles of an Nb/C/Nb trilayer structure investigated at different locations (1, 2, 3, . . . , 6) on the sample surface. We used a focused X-ray beam of energy $E = 12$ keV from kinoform lens optics and performed the XRR measurements in sample scanning mode. The inset indicates the different locations for XRR measurement on the Nb/C/Nb sample surface as marked by the numbers. Each point was separated by 2 mm.

compared with Be CRL optics, as these lenses are usually fabricated on a high-Z substrate (Si or Ge). Owing to the small footprint of the focused beam on the sample surface, the diffused scattered background seen by the detector, in the specular reflected beam, is significantly small. The small physical dimension of a kinoform structure makes it possible to fabricate several lenses for different X-ray energies and/or different focal lengths on a single Si chip. Thus, it is easy to change the photon energy by just a lateral translation of the lens chip, without changing the focal distance. Apart from the above advantages, the focused beam from a kinoform is divergent in nature; therefore one needs to take into account the beam divergence effect during XRR calculation/fitting of experimental data. For example, in our case, during the XRR fit we employed a beam divergence of $\sim 0.02^\circ$ (0.009°) at an X-ray energy of 12 keV (19 keV). These values of primary beam divergence were obtained using geometrical calculations from the focal distance and effective aperture of the kinoform lens structures at given X-ray energy. The effective aperture of a kinoform lens decreases with increasing X-ray energy (Alianelli *et al.*, 2009), therefore the observed beam divergence of the kinoform lens also decreases at higher X-ray energies. Thus, kinoform lenses are especially useful in performing XRR measurements of thin layered materials at higher incident X-ray energies.

4. Conclusions

We have presented X-ray reflectivity measurements of thin layered structures using focused X-ray beams generated from kinoform lens structures. The results obtained show that such focused X-ray beams can easily be employed for microstructural characterization of thin layered materials using XRR measurements. Various advantages of kinoform lenses, such as a line-shaped focused X-ray beam, high X-ray transmission efficiency and low scattered background, make them ideal for XRR applications, especially at higher incident X-ray energies. Moreover, the small footprint of the X-ray beam at grazing incidence angle also offers another possibility of performing XRR analysis in sample scanning mode. Such measurements are very useful in investigating the degree of homogeneity of thin layered materials, for example X-ray multilayer structures or planar thin film X-ray waveguide structures coated on plane or curved-shaped substrates.

This work was carried out with the support of Diamond Light Source. The kinoform lenses used in this work were fabricated using funding from STFC facility development grant STFC/F001665/1. The technical support of Andrew Malandain for the experiment set-up is acknowledged. We also thank M. Nayak and G. S. Lodha for providing the multilayer samples.

References

Alianelli, L., Sawhney, K. J. S., Jenkins, D. W. K., Loader, I. M., Stevens, R., Snigirev, A. & Snigireva, I. (2007). *Proc. SPIE*, **6705**, 670507.
Alianelli, L., Sawhney, K. J. S., Tiwari, M. K., Dolbnya, I. P., Stevens, R., Jenkins, D. W. K., Loader, I. M., Wilson, M. C. & Malik, A. (2009). *J. Synchrotron Rad.* **16**, 325–329.
Barbee, T. W. (1985). *Synthetic Modulated Structure Materials*, p. 313. New York: Academic.
Cedola, A., Stanic, V., Burghammer, M., Lagomarsino, S., Rustichelli, F., Giardino, R., Aldini Nicoli, N. & Di Fonzo, S. (2003). *Phys. Med. Biol.* **48**, N37–N48.
Costa, A. T. Jr, de Castro Barbosa, A. C., d'Albuquerque e Castro, J. & Muniz, R. B. (2001). *J. Phys. Condens. Matter*, **13**, 1827–1837.
Di Fonzo, S., Jark, W., Lagomarsino, S., Giannini, C., De Caro, L., Cedola, A. & Müller, M. (2000). *Nature (London)*, **403**, 638–640.
Drakopoulos, M., Zegenhagen, J., Snigirev, A., Snigireva, I., Hauser, M., Eberl, K., Aristov, V., Shabelnikov, L. & Yunkin, V. (2002). *Appl. Phys. Lett.* **81**, 2279–2281.
Evans-Lutterodt, K., Ablett, J., Stein, A., Kao, C., Tennant, D., Klemens, F., Taylor, A., Jacobsen, C., Gammel, P., Huggins, H., Bogart, G., Ustin, S. & Ocola, L. (2003). *Opt. Express*, **11**, 919–926.
Isakovic, A. F., Stein, A., Warren, J. B., Narayanan, S., Sprung, M., Sandy, A. R. & Evans-Lutterodt, K. (2009). *J. Synchrotron Rad.* **16**, 8–13.
Jark, W., Cedola, A., Di Fonzo, S., Fiordelisi, M., Lagomarsino, S., Kovalenko, N. V. & Chernov, V. A. (2001). *Appl. Phys. Lett.* **78**, 1192–1194.
Lagomarsino, S., Cedola, A., Cloetens, P., Di Fonzo, S., Jark, W., Souillie, S. & Riekel, C. (1997). *Appl. Phys. Lett.* **71**, 2557–2559.
Lodha, G. S. (2009). *RRCAT Newsl.* **22**, 7.
Matsui, J., Fukuda, K., Kamakura, A., Tsusaka, Y., Kagoshima, Y., Toyoda, N. & Yamada, I. (2007). *Nucl. Instrum. Methods Phys. Res. B*, **261**, 634–638.
Parratt, L. G. (1954). *Phys. Rev.* **95** 359–369.
Reichert, H., Honkimaki, V., Snigirev, A., Engemann, S. & Dosch, H. (2003). *Physica B*, **336**, 46–55.
Revaz, B., Cyrille, M. C., Zink, B. L., Schuller, I. K. & Hellman, F. (2002). *Phys. Rev. B*, **65**, 094417.
Sawhney, K. J. S., Dolbnya, I. P., Tiwari, M. K., Alianelli, L., Scott, S. M., Preece, G. M., Pedersen, U. K. & Walton, R. D. (2009). *Proceedings of the Tenth International Conference on Synchrotron Radiation Instrumentation.* In the press.
Snigirev, A., Kohn, V., Snigireva, I. & Lengeler, B. (1996). *Nature (London)*, **384**, 49–51.
Spiller, E. (1972). *Appl. Phys. Lett.* **20**, 365.
Stein, A., Evans-Lutterodt, K., Bozovic, N. & Taylor, A. (2008). *J. Vac. Sci. Technol. B*, **26**, 122–127.
Tiwari, M. K., Naik, S. R., Lodha, G. S. & Nandedkar, R. V. (2005). *Anal. Sci.* **21**, 757–762.
Wellock, K., Theeuwen, S. J. C. H., Caro, J., Gribov, N. N., van Gorkom, R. P., Radelaar, S., Tichelaar, F. D., Hickey, B. J. & Marrows, C. H. (1999). *Phys. Rev. B*, **60**, 10291–10301.
Windt, D. L., Donguy, S., Hailey, C. J., Koglin, J., Honkimaki, V., Ziegler, E., Christensen, F. E., Chen, H., Harrison, F. A. & Craig, W. W. (2003). *Appl. Opt.* **42**, 2415–2421.
Wolkenhauer, M., Bumbu, G. G., Cheng, Y., Roth, S. V. & Gutmann, J. S. (2006). *Appl. Phys. Lett.* **89**, 054101.
Zahn, P., Papanikolaou, N., Erler, F. & Mertig, I. (2002). *Phys. Rev. B*, **65**, 134432.
Zwanenburg, M. J., Peters, J. F., Bongaerts, J. H. H., de Vries, S. A., Abernathy, D. L. & van der Veen, J. F. (1999). *Phys. Rev. Lett.* **82**, 1696–1699.